Journal of Computational Physics 228 (2009) 5722–5739

Contents lists available at ScienceDirect

Journal of Computational Physics

journal homepage: www.elsevier.com/locate/jcp

An all-speed relaxation scheme for interface flows with surface tension

Benjamin Braconnier [a,c,*], Boniface Nkonga [b,c]

[a] Glaizer Group: Générateur de Technologies Innovantes, 32 rue Guy Moquet, 92240 Malakoff, France
[b] Laboratoire J.A. Dieudonné, U.M.R. C.N.R.S. No. 6621, Université de Nice Sophia-Antipolis, Parc Valrose, 06108 Nice Cedex 02, France
[c] MAB, Univ. Bordeaux 1/INRIA Futurs, ScAlApplix 351 cours de la libération, 33400 Talence, France

ARTICLE INFO

Article history:
Received 26 August 2008
Received in revised form 10 April 2009
Accepted 27 April 2009
Available online 15 May 2009

Keywords:
Compressible fluid
Multi-phase flow
Diffuse interface method
Surface tension
Relaxation scheme
Non-conservative system
Low Mach preconditioning
Implicit scheme

ABSTRACT

We consider interface flows where compressibility and capillary forces (surface tension) are significant. These flows are described by a non-conservative, unconditionally hyperbolic multiphase model. The numerical approximation is based on finite-volume method for unstructured grids. At the discrete level, the surface tension is approximated by a volume force (CSF formulation). The interface physical properties are recovered by designing an appropriate linearized Riemann solver (Relaxation scheme) that prevents spurious oscillations near material interfaces. For low-speed flows, a preconditioning linearization is proposed and the low Mach asymptotic is formally recovered. Numerical computations, for a bubble equilibrium, converge to the required Laplace law and the dynamic of a drop, falling under gravity, is in agreement with experimental observations.

0. Introduction

Modeling and computing multi-fluid flows is a very active research area. This is due to the fact that multi-fluid flows play fundamental roles in many natural phenomena used in industrial process. The diversity of the characteristic scales in one phenomena leads to large difficulties when numerical simulation is considered. Although the constant evolution of computational resources enables finest resolutions, numerical methods accuracy and efficiency always need to be improved.

There are two main difficulties specific to interfaces flows: the interface shape dynamic and the wave transmission. *Interface tracking* approaches use an explicit definition of the interface. The *front tracking method* [17] uses a lower dimensional grid to represent interfaces in numerical solutions. Propagation of the front is obtained by the requirement of jumps conditions. For the *Volume of Fluid* [38] method, the interface is described by an average fluid fraction function and the interface is reconstructed by different approaches. The main difficulties of these methods are related to shape topology changes and they are not well adapted for multiple interfaces flows such as sprays. The *level set* method [15] overcomes these difficulties by embedding interfaces in a distance function. Unfortunately, although many recent works deal with accurate wave transmission (GFM [15], SFM [2]), multidimensional and unstructured grid extension needs to be improved [32]. An other way to overcome the difficulties related to sharp interfaces is to artificially smooth the interface (*diffuse interface methods*) and create a mixture zone such as to recover the physical properties of the sharp interface. This leads generally to non-conservative hyperbolic models [5,29] for which the weak solutions of finite volume approximations are not well defined. Nevertheless, the relevance of this method has been successfully proved in [37] for inviscid high speed flows. Surface tension

* Corresponding author. Address: Glaizer, 32 rue Guy Moquet, 92240 Malakoff, France.
E-mail addresses: benjamin.braconnier@glaizer.com (B. Braconnier), boniface.nkonga@unice.fr (B. Nkonga).

0021-9991/$ - see front matter © 2009 Elsevier Inc. All rights reserved.
doi:10.1016/j.jcp.2009.04.046

forces has been considered in [35] and the low mach preconditioning in [20]. For theses works, the discrete non-conservative operators are obtained by the inversion of well balanced relations [1].

In the context of diffuse interface method, this paper focus on computations of low Mach interface flows submitted to surface tensions forces. The physical model is based on the five equation model [29,33], a simplified version of the Baer Nunziato model [5]. As the interface is not sharply defined, the capillary effects are formulated by a *Continuum Surface Force* (CSF [9]) which uses a color function. The finite volume approximation is formulated in terms of local fluctuations deduced from the approximate resolution of Riemann problems. Indeed, in order to reduce the currently observed parasitic currents [27], the surface tension terms needs to be considered as part of the non-conservative hyperbolic subsystem. This non-conservative formulation must be preserved [16,30] in order to avoid wrong discontinuous solutions [24]. Its resolution needs the definition of regularizing viscous paths [16] or the elaboration of kinetic relations [23]. Despite, when the surface tension forces model relies on a color function constant across shock and rarefaction waves, surface tension terms can be reformulated in a conservative form [18]. In [35], a numerical scheme based on a Godunov method is proposed for this specific case. It formally and numerically recovers the Laplace law and enable the computation of complex interface flows. Unfortunately, it can not be easily generalized to the system [29] which volume fraction equation is not a simple transport equation or when complex equations of state are considered. In [3,33], balance equations between conservative and non-conservative terms are pointed out in order to derive consistent discrete non-conservative operators [1]. The major drawback of this method is its complexity when the model include too many non-conservative operators. In our work, we propose an approximate Riemann solvers based on the relaxation scheme [12,28,31,39,14] which yields an implicit viscous regularization of non-conservative operators. Thus, fluctuations are evaluated by the virtue of a linearized non-conservative Riemann problem that takes into account surface tension force as a first order derivative. Their expressions are analytically formulated and without thermodynamical parameters. The resulting scheme is thus very efficient. Moreover, considering asymptotic expansions, we formally prove that the non-conservative operator regularization is consistent with the mathematical model. Then, using the pressure as an independent variable in the relaxation scheme gives a natural way to propose a low Mach preconditioning by the introduction of the times scales related to the acoustic and the material waves.

The paper is organized as follows. We describe, in Section 1, the governing equations. In Section 2, the finite volume approximation is defined. A relaxation system is proposed for the physical model and the solution of the associated Riemann problem is constructed. The main numerical scheme is then achieved. Section 3 is devoted to the presentation of some specific numerical tools: low Mach preconditioning, surface tension approximation and implicit schemes. In Section 4, we discuss the numerical results obtained for a bubble at equilibrium under the Laplace law, shock bubble interactions and a falling water drop. In the last section, we propose discussions of the achievement and draw inferences for further work.

1. Mathematical model

Let us consider a multi-phase flow and use the subscript k for the specification of each component. The physical model considered in this paper assumes that pressures and velocities are at equilibrium. The physical model, obtained as an asymptotic limit of the non-equilibrium Baer–Nunziato system [5], is given by a single pressure and velocity multi-phase flow [29,19]:

$$\begin{cases} \partial_t(\alpha_k) + \mathbf{u}\cdot\nabla(\alpha_k) - \beta_k\nabla\cdot(\mathbf{u}) = 0, \\ \partial_t(\alpha_k\rho_k) + \nabla\cdot(\alpha_k\rho_k\mathbf{u}) = 0, \\ \partial_t(\rho\mathbf{u}) + \nabla\cdot(\rho\mathbf{u}\otimes\mathbf{u} + p) = \nabla\cdot(\tau) + \mathbf{f}_S + \rho\mathbf{g}, \\ \partial_t(E) + \nabla\cdot(\rho H\mathbf{u}) = \nabla\cdot(\tau\mathbf{u}) + \mathbf{u}\cdot(\mathbf{f}_S + \rho\mathbf{g}) - \nabla\cdot(\mathbf{q}), \end{cases} \tag{1}$$

where ρ is the mixture density, $\mathbf{u}$ is the fluid velocity, E the total energy, p the pressure and H the enthalpy. For each component, α_k is the volume fraction, ρ_k is the partial density, $\varepsilon_k = \varepsilon_k(\rho_k, p)$ is the partial internal energy. The mixture density, internal energy, total energy and the enthalpy are defined as:

$$\rho = \sum_k \alpha_k\rho_k, \quad \rho\varepsilon = \sum_k \alpha_k\rho_k\varepsilon_k, \quad E = \rho\varepsilon + \frac{1}{2}\rho\mathbf{u}\cdot\mathbf{u}, \quad H = \frac{E+p}{\rho}.$$

We assume that the equation of state associated to each component is governed by the stiffened gas EOS: $p(\rho_k, \varepsilon_k) = (\gamma_k - 1)(\rho_k\varepsilon_k - \rho_k\varepsilon_k^\infty) - \gamma_k p_k^\infty$, where ε_k^∞ and p_k^∞ are fixed reference thermodynamic states. The perfect gas EOS is recovered when $\varepsilon_k^\infty = p_k^\infty = 0$. According to the pressure equilibrium and the constraint of entropy conservation along phase trajectories [19], the pressure p is a combination of the equation of state associated to the components of the flow:

$$\frac{p + \gamma p^\infty}{\gamma - 1} = \rho(\varepsilon - \varepsilon^\infty), \tag{2}$$

where the mixture parameters γ, p^∞ and ε^∞ depends on the volume fraction and are defined by the relations:

$$\frac{1}{\gamma - 1} = \sum_k \frac{\alpha_k}{\gamma_k - 1}, \quad \frac{\gamma p^\infty}{\gamma - 1} = \sum_k \frac{\alpha_k\gamma_k p_k^\infty}{\gamma_k - 1} \quad \text{and} \quad \rho\varepsilon^\infty = \sum_{k=1}^{q} \alpha_k\rho_k\varepsilon_k^\infty. \tag{3}$$

For each pure fluid the speed of sound c_k is defined as:

$$c_k = \sqrt{\left.\frac{\partial p}{\partial \rho_k}\right|_{S_k}},$$

where S_k is the pure fluid entropy.

In the volume fraction equation, β_k is a function that takes into account the volume variations due to compression or expansion processes. According to the asymptotic regime under consideration, two different formulations can be found with their associated mixture speed of sound c:

- When partial pressures fluctuations are assumed very small, the asymptotic equations derived from the Baer–Nunziato model give [33]

$$\beta_k = 0 \quad \text{and} \quad c^2 = (\gamma - 1)\left(\sum_k \frac{\alpha_k \rho_k c_k^2}{\gamma_k - 1}\right). \tag{4}$$

- When the first order fluctuations of partial pressures are considered, the derived asymptotic model is defined with [29,19]

$$\beta_k = \alpha_k\left(1 - \frac{\rho c^2}{\rho_k c_k^2}\right) \quad \text{and} \quad \frac{1}{\rho c^2} = \sum_k \frac{\alpha_k}{\rho_k c_k^2}. \tag{5}$$

In the present model, even if velocities and pressures equilibrium is assumed, there is no temperature equilibrium. Partial temperatures T_k are given by:

$$p + p_k^\infty = (\gamma_k - 1)\rho_k^{\gamma_k} C_{vk}\left(\frac{T_k}{\rho_k^{\gamma_k - 1}} - \frac{T_k^\infty}{\rho_{k0}^{\gamma_k - 1}}\right), \tag{6}$$

where C_{vk}, ρ_{k0} and T_k^∞ are thermodynamic parameters (assumed constant for simplicity). The effective heat flux vector $\mathbf{q}$ is the sum of partial-heat conduction approximated by Fourier's law:

$$\mathbf{q} = -\sum_k \alpha_k \lambda_k \nabla T_k,$$

where λ_k is the thermal conductivity associated to the fluid k. The viscosity effects are modeled by the following 'mixture' viscosity stress tensor:

$$\tau = \mu\left(\nabla \mathbf{u} + \nabla \mathbf{u}^T - \frac{2}{3}\nabla \cdot \mathbf{u}\right) \quad \text{with} \quad \frac{1}{\mu} = \sum_k \frac{\alpha_k}{\mu_k}, \tag{7}$$

where μ_k is the viscosity coefficient associated to the fluid k and μ is the effective viscosity coefficient.

Source terms are the contribution of external forces: the gravity $\rho \mathbf{g}$ and the surface tension forces $\mathbf{f}_S$ localized on the interfaces. For a point $\mathbf{x}_{kk'}$ of the interface between the fluid k and the fluid k', the tension force is defined as

$$\mathbf{f}_S(\mathbf{x}_{kk'}) = -\sigma_{kk'}\kappa(\mathbf{x}_{kk'})\boldsymbol{n}(\mathbf{x}_{kk'}), \tag{8}$$

where $\sigma_{kk'}$ is a characteristic coefficient depending on the fluids nature, $\boldsymbol{n}(\mathbf{x}_{kk'})$ and $\kappa(\mathbf{x}_{kk'})$ are respectively the normal and the curvature at the point $\mathbf{x}_{kk'}$. This formulation is not adapted to numerical strategies where interfaces are not explicitly tracked. In practice, we will consider a "Continuum Surface Force" (CSF) formulation discussed in [9,35]. The first step of this modeling is the introduction of a smooth level-set function $\Gamma_{kk'}$ defined around the interface, varying from 1 in the fluid k to 0 in the fluid k'. This function is constructed from the local quantities with strategies that usually use complex operators. For the sake of simplicity, we assume that the level-set function is locally transported at the flow velocity [15]:

$$\partial_t(\Gamma_{kk'}) + \mathbf{u} \cdot \nabla(\Gamma_{kk'}) = 0. \tag{9}$$

Therefore, the surface tension force is represented as a continuum force per unit volume in regions along and near the interface [9]:

$$\mathbf{f}_S \simeq -\sigma_{kk'}\kappa_{kk'}\nabla\Gamma_{kk'} \quad \text{where} \quad \kappa_{kk'} = \kappa(\Gamma_{kk'}) = \nabla \cdot \left(\frac{\nabla\Gamma_{kk'}}{|\nabla\Gamma_{kk'}|}\right). \tag{10}$$

For simplicity in the sequel, the interface function and its coefficients will be denoted with only one index. As the surface tension is expressed with differential operators, it will be considered as part of the propagation operators of the system (1). Let us note that a conservative formulation of this force is very attractive when the volume fraction obeys a transport equation ($\beta_k = 0$) [35]. As the system (1) is more complex, this formulation will not be considered here.

1.1. Mathematical model reformulation in view of numerical approximation

In order to design the numerical approximation, the physical model is reformulated as follows:

$$\partial_t(\mathbf{W}) + \nabla\cdot(\mathbf{F}) + \mathbf{B}\nabla\mathbf{V} = \nabla\mathscr{R}(\nabla\mathbf{V}) + \mathscr{S}, \tag{11}$$

where $\mathbf{W} = \mathbf{W}(t,\mathbf{x})$ is the state vector for $t \in]0,T]$ and $\mathbf{x} \in \Omega$ with T the final time and Ω the domain of the study. $\mathbf{F} = \mathbf{F}(\mathbf{W},p)$ denotes the conservative components of the convection flux. These vectors are defined as:

$$\mathbf{W} = \begin{pmatrix} \alpha_k \\ \alpha_k\rho_k \\ \rho\mathbf{u} \\ E \\ \Gamma_k \end{pmatrix}, \quad \mathbf{F} = \mathbf{F}(\mathbf{W},p) = \begin{pmatrix} 0 \\ \alpha_k\rho_k\mathbf{u} \\ \rho\mathbf{u}\otimes\mathbf{u} + p \\ (E+p)\mathbf{u} \\ 0 \end{pmatrix}.$$

The matrix $\mathbf{B}$ is associated to the non-conservative contributions and contains the terms related to volume variations in compression or expansion processes and the CSF modeling of the surface tension forces:

$$\mathbf{V} = \begin{pmatrix} \alpha_k \\ \alpha_k\rho_k \\ \mathbf{u} \\ p \\ \Gamma_k \end{pmatrix}, \quad \mathbf{B}\nabla\mathbf{V} = \begin{pmatrix} \mathbf{u}\cdot\nabla(\alpha_k) - \beta_k\nabla\cdot(\mathbf{u}) \\ 0 \\ \sigma_k\kappa_k\nabla\Gamma_{kk'} \\ \sigma_k\kappa_k\mathbf{u}\cdot\nabla\Gamma_{kk'} \\ \mathbf{u}\cdot\nabla\Gamma_{kk'} \end{pmatrix}$$

Viscous and heat fluxes are second order derivatives contributions resumed by $\nabla\mathscr{R}(\nabla\mathbf{V})$. The source term $\mathscr{S}$ is associated to external forces and eventually to additional physics related to geometrical considerations. Indeed, let us assume a 2D axisymmetrical flow and identify the distance r from the symmetric axis to the coordinate y ($y \equiv r$). Then, according to the domain perturbation technique, the flow can be computed with a 2D formulation by adding the specific contribution to the source term $\mathscr{S}$:

$$\frac{1}{r}(\mathbf{F}\cdot\mathbf{e}_r) + \frac{1}{r}\begin{pmatrix} \beta_k\mathbf{u}\cdot\mathbf{e}_r \\ 0 \\ 0 \\ 0 \\ 0 \end{pmatrix} + \frac{1}{r}\frac{\nabla(\Gamma_k)\cdot\mathbf{e}_r}{|\Gamma_k|}\cdot\begin{pmatrix} 0 \\ 0 \\ \nabla\Gamma_k \\ \mathbf{u}\cdot\nabla\Gamma_k \\ 0 \end{pmatrix}.$$

where $\mathbf{e}_r$ is the unit vector in the direction $r \equiv y$.

The major numerical difficulties related to the resolution of the system (11) are due to the first order derivative subsystem (left hand size) and to the non-conservative nature of the model. The mathematical analysis shows that, under the constitutive laws (2) and (3), the first order system is hyperbolic with the characteristic velocities $\mathbf{u}\cdot\boldsymbol{n} - c$, $\mathbf{u}\cdot\boldsymbol{n}$ and $\mathbf{u}\cdot\boldsymbol{n} + c$ when projected along the direction $\boldsymbol{n}$. The speed of sound c obeys (4) or (5), depending on the considered asymptotic model. The wave $\mathbf{u}\cdot\boldsymbol{n}$ is linearly degenerated and, for constant curvature κ_k, admits the Riemann invariants $\mathbf{u}\cdot\boldsymbol{n}$ and $p + \sigma_k\kappa_k\Phi_k$. Therefore, the pressure can be discontinuous across a material interface and the Laplace law is locally recovered.

2. Finite volume approximations

We consider a non-overlapping conformal partition of Ω into vertex-centered control volumes C_i (see Fig. 1). These volumes are closed and can be decomposed in non-overlapping sub zonal cells C_{ij} associated to neighbor cells C_i and C_j:

$$\Omega \simeq \bigcup_{i=1}^{Ns} C_i, \quad C_i = \bigcup_{j\in\vartheta(i)} C_{ij},$$

where $j \in \vartheta(i)$ when C_i and C_j are neighbor cells.

The finite volume approximation is obtained by integrating the system (11) over a space-time cell $Q_i = [t^n, t^{n+1}] \times C_i$:

$$a_i(\mathbf{W}_i^{n+1} - \mathbf{W}_i^n) + \int_{t^n}^{t^{n+1}}\int_{C_i}(\nabla\cdot\mathbf{F} + \mathbf{B}\nabla\mathbf{V}) = \int_{t^n}^{t^{n+1}}\int_{C_i}(\nabla\mathscr{R}(\nabla\mathbf{V}) + \mathscr{S}),$$

where a_i is the volume of the cell and $\mathbf{W}_i$ is an average state defined as

$$\mathbf{W}_i(t) = \frac{1}{a_i}\int_{C_i}\mathbf{W}(t,\mathbf{x})d\mathbf{x}.$$

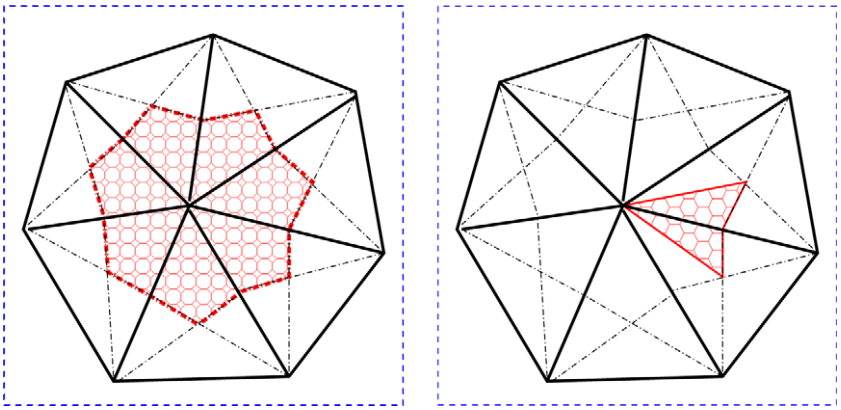

Fig. 1. 2D mesh of triangles: construction of the cell C_i centered at a mesh vertex (left) and of the corner sub-cell C_{ij} associated to two neighbor vertices (right).

The discrete form of diffusive fluxes is achieved by the finite volume/finite elements equivalence and the source terms are approximated following a standard splitting technique:

$$\int_{t^n}^{t^{n+1}} \int_{C_i} \nabla \mathscr{R}(\nabla \mathbf{V}) \simeq \Delta t \sum_{j\in\vartheta(i)} \boldsymbol{\varphi}_{ij} \quad \text{and} \quad \int_{t^n}^{t^{n+1}} \int_{C_i} \mathscr{S} \simeq \Delta t a_i \boldsymbol{S}_i,$$

where $\Delta t = t^{n+1} - t^n$. For explicit schemes, $\mathscr{R}_{ij}$ and $\mathscr{S}_i$ will be evaluated at the time t^n and at the time t^{n+1} for implicit schemes.

The approximation of first order spatial derivatives is not classical. Indeed, the non-conservative contributions cannot be formulated as fluxes balance on cell boundaries. In the present paper, we propose the use of relaxation solvers [28,14] to perform those approximations. In order to achieve this task, we define a sub zonal state $\mathbf{W}_{i,j}$ such as

$$\mathbf{W}_{i,j} = \frac{1}{a_{i,j}} \int_{C_{i,j}} \mathbf{W} dx \quad \text{and} \quad a_i \mathbf{W}_i = \sum_{j\in\vartheta(i)} a_{i,j} \mathbf{W}_{i,j},$$

where $a_{i,j}$ is the volume of the sub-cell $C_{i,j}$. The numerical scheme associated to $\mathbf{W}_{i,j}$ writes as

$$a_{i,j} \frac{\mathbf{W}_{i,j}^{n+1} - \mathbf{W}_{i,j}^{n}}{\Delta t} + \boldsymbol{\psi}_{i,j} = \boldsymbol{\varphi}_{i,j} + a_{i,j} \boldsymbol{S}_i, \tag{12}$$

where the fluctuation $\boldsymbol{\psi}_{i,j} = \boldsymbol{\psi}_{i,j}(\mathbf{W}_i, \mathbf{W}_j)$ is given by

$$\boldsymbol{\psi}_{i,j} = \frac{1}{\Delta t} \left(\int_{t^n}^{t^{n+1}} \int_{\partial C_{i,j}} \mathbf{F} \cdot \boldsymbol{n}_{i,j} \, ds dt + \int_{t^n}^{t^{n+1}} \int_{C_{i,j}} \mathbf{B} \nabla \mathbf{V} \, dx dt \right),$$

where $\boldsymbol{n}_{i,j}$ is the outgoing (of the cell i) unit normal. Proper approximation of this fluctuation have to preserve some asymptotic of this system, by a well balance of numerical viscosity between the conservative and the non-conservative components [3,33]. Let us consider the following Riemann problem associated to the direction $\boldsymbol{n}$ with the initial states $\mathbf{W}_i^n$ and $\mathbf{W}_j^n$ and use the associated coordinate ξ:

$$\begin{cases} \partial_t \mathbf{W} + \partial_\xi (\mathbf{F} \cdot \boldsymbol{n}) + (\mathbf{B} \cdot \boldsymbol{n}) \partial_\xi (\mathbf{V}) = 0, \\ \mathbf{W}(t^n, \xi) = \begin{cases} \mathbf{W}_i \text{ if } \xi < \xi_{ij}, \\ \mathbf{W}_j \text{ if } \xi > \xi_{ij}. \end{cases} \end{cases} \tag{13}$$

If $\mathscr{V}(t, \mathbf{x}, \boldsymbol{n}, \xi_{ij}, \mathbf{W}_i, \mathbf{W}_j)$ is a the solution of (13) (see [16,30]), then a compatible fluctuation can be obtained by an extension of the Godunov technique to multidimensional computation

$$\boldsymbol{\psi}_{i,j} = \frac{1}{\Delta t} \int_{C_{i,j}} [\mathbf{W}_i - \mathscr{V}(t^{n+1}, \mathbf{x}, \boldsymbol{n}_{ij}, \xi_{ij}, \mathbf{W}_i, \mathbf{W}_j)] \, dx,$$

where $\boldsymbol{n}_{ij}$ and ξ_{ij} are fixed. In practice, we use an approximation that preserves the properties of the initial scheme:

$$\boldsymbol{\psi}_{i,j} \approx |\boldsymbol{\eta}_{i,j}| \int_{-\alpha_{ij}}^{0} [\mathbf{W}_i^n - \mathscr{V}_{i,j}(\sigma)] \, d\sigma, \quad \text{where} \quad \sigma(\mathbf{x}) = \frac{\mathbf{x} \cdot \boldsymbol{n}_{ij} - \xi_{ij}}{t^{n+1} - t^n},$$

$$\boldsymbol{\eta}_{i,j} = \int_{\partial C_{i,j}} \boldsymbol{n}_{i,j} \, ds \quad \text{and, for consistency,} \quad \alpha_{ij} = \frac{a_{i,j}}{\Delta t |\boldsymbol{\eta}_{i,j}|}.$$

The system (13) is unconditionally hyperbolic and the associated eigenvalues are $\lambda_{-c} = \boldsymbol{u}\cdot\boldsymbol{n} - c$, $\lambda_u = \boldsymbol{u}\cdot\boldsymbol{n}$ and $\lambda_{+c} = \boldsymbol{u}\cdot\boldsymbol{n} + c$ where λ_{-c} and λ_{+c} are associated to genuinely nonlinear waves. This makes difficult the resolution of the Riemann problem for this system. In order to overcome this difficulty, we propose in the next section to design an approximate Riemann solver for the current non-conservative system, such as to well balance the numerical dissipation.

2.1. Relaxation scheme for a non-conservative hyperbolic system

Relaxation schemes are well established tools for the numerical approximation of fluid flows [28,14,7]. The main principle of these schemes is to design a perturbed system, simple to solve, which solutions are a dissipative limit of the original system solutions. This technique was initially designed for conservative systems [28]. In this specific context, there is an equivalence [8] with the HLLC schemes [42]. Unlike the HLLC, the relaxation is a very attractive strategy for the resolution of systems with non-conservative operators [6,7] or with severe nonlinearities.

The most difficult task in the design of relaxation schemes is to derive an extended system of the form

$$\partial_t \mathbf{W}_\lambda + \partial_\xi \mathscr{F}_\lambda + \mathscr{B}_\lambda \partial_\xi \mathbf{V}_\lambda = \frac{1}{\lambda}\mathbf{R}_\lambda, \tag{14}$$

where the augmented variable $\mathbf{W}_\lambda$ contains the components of $\mathbf{W}$ and some additional independent variables. $\partial_\xi \mathscr{F}_\lambda$ and $\mathscr{B}_\lambda \partial_\xi \mathbf{V}_\lambda$ are the augmented conservative and non-conservative contributions. The operator $\mathbf{R}_\lambda$ is used to relax $\mathbf{W}_\lambda$ toward $\mathbf{W}$, when λ goes to zero and make the initial system a dissipative limit of the relaxation system (14). The relaxation strategy is achieved in two steps: the evolution and the projection.

The evolution is devoted to the resolution of the following system:

$$\partial_t \mathbf{W}_\lambda + \partial_\xi \mathbf{F}_\lambda + \mathbf{B}_\lambda \partial_\xi \mathbf{V}_\lambda = 0. \tag{15}$$

In order to make the strategy attractive, the Riemann problem associated to this system should be easy to compute. In practice, we will define the relaxation system such that (15) is linearly degenerated and the Riemann invariants can be computed. Thus, the solution of the associated Riemann problem is piecewise constant, and for a given eigenvalue ordering, is fully defined by the system of invariants.

In the projection step, a set of ordinary differential equations is solved:

$$\partial_t \mathbf{W}_\lambda = \frac{1}{\lambda}\mathbf{R}_\lambda. \tag{16}$$

Its solution is the projection of the augmented variables $\mathbf{W}_\lambda$ on the equilibrium manifold $\mathbf{W}$.

For the Euler system, a linearized pressure π is used as additional variable and is governed by the equation:

$$\partial_t(\pi) + u\partial_\xi(\pi) + \frac{a^2}{\rho}\partial_\xi(u) = \frac{1}{\lambda}(p-\pi),$$

where $u = \mathbf{u}\cdot\boldsymbol{n}$ and a is a parameter that controls the numerical dissipation of the scheme [8]. In this case, the relaxation scheme can be viewed as a linear approximation of the Hugoniot relation under steady flow assumption.

In the present work, we propose a relaxation system obtained by introducing three additional variables: Φ_k the interface function, π a linearized pressure and θ_k a measure of impedance fluctuations. The augmented system is defined by:

$$\begin{cases} \partial_t \alpha_k + u\partial_\xi \alpha_k + \alpha_k\left(1 - \frac{\rho_k}{\rho}\theta_k^2\right)\partial_\xi u = 0, \\ \partial_t(\alpha_k\rho_k) + \partial_\xi(\alpha_k\rho_k u) = 0, \\ \partial_t(\rho u) + \partial_\xi(\rho u^2 + \pi) + \sigma_k\kappa_k\partial_\xi\Phi_k = 0, \\ \partial_t E + \partial_\xi((E+\pi)u) + \sigma_k\kappa_k u\partial_\xi\Phi_k = 0, \\ \partial_t\Phi_k + u\partial_\xi\Phi_k = \frac{1}{\lambda}(\Phi_k - \Gamma_k(\mathbf{V})), \\ \partial_t\pi + \left(u + \frac{a^R - a^L}{\rho}\right)\partial_\xi\pi + \frac{a^L a^R}{\rho}\partial_\xi u = \frac{1}{\lambda}(p-\pi), \\ \partial_t(\theta_k^2) + u\partial_\xi(\theta_k^2) = \frac{1}{\lambda}(r_k^2 - \theta_k^2), \end{cases} \tag{17}$$

where $r_k^2 = \frac{\rho}{\rho_k}\left(1 - \frac{\beta_k}{\alpha_k}\right)$ such that $\alpha_k\left(1 - \frac{\rho_k}{\rho}\theta_k^2\right)$ will relax to β_k. The parameters a^L and a^R control the numerical viscosity of the approximation. The introduction of the interface function Φ_k makes the relaxation system suitable for any type of level-set function even if the advection Eq. (9) is not considered. In particular, this new variable overcomes some difficulties when $\Gamma_k(\mathbf{V})$ is a complex nonlinear function of $\mathbf{V}$. If we assume that the curvature is locally constant, we can derive an exact solution of the Riemann problem for the augmented system. Indeed, in this case, the system (17) is unconditionally hyperbolic. The characteristic velocities, $u - a^L/\rho, u$ and $u + a^R/\rho$ are linearly degenerated. The associated Riemann invariants are given in the following table:

wave	Riemann invariants						
$u-\frac{a^L}{\rho}$	$u-\frac{a^L}{\rho}$	$\pi+a^Lu$	$\pi^2-2(a^L)^2\varepsilon$	$\frac{\alpha_k\rho_k}{\rho}$	Φ_k	θ_k^2	I_7
u	u			$\pi+\sigma_k\kappa_k\Phi_k$			
$u+\frac{a^R}{\rho}$	$u+\frac{a^R}{\rho}$	$\pi-a^Ru$	$\pi^2-2(a^R)^2\varepsilon$	$\frac{\alpha_k\rho_k}{\rho}$	Φ_k	θ_k^2	I_7

(18)

where $I_7=(\alpha_k-\theta_k^2\frac{\alpha_k\rho_k}{\rho})/\rho$ for the Kapila model and $I_7=\alpha_k$ for the Massoni model. The exact solution of the Riemann problem is piecewise constant and the Riemann invariants give an invertible system to compute intermediate quantities. Initial left and right values are p^L and p^R for π, r_k^L or r_k^R for θ_k and $\Gamma_k(\mathbf{V}^L)$ and $\Gamma_k(\mathbf{V}^R)$ for Φ_k.

In order to exhibit this analytic solution, let us introduce the reals $a^{L,1}, a^{L,2}, a^{R,1}$ and $a^{R,2}$ defined by:

$$\begin{cases} a^{L,1}=max(-\rho^L\Delta u,0),\\ a^{R,1}=max(-\rho^R\Delta u,0),\\ a^{L,2}=\sqrt{max(\rho^L(\Delta p+\sigma_k\kappa_k\Delta\Phi_k)-a^{R,1}(a^{L,1}+\rho^L\Delta u),0)},\\ a^{R,2}=\sqrt{max(-\rho^R(\Delta p+\sigma_k\kappa_k\Delta\Phi_k)-a^{L,1}(a^{R,1}+\rho^R\Delta u),0)}. \end{cases} \tag{19}$$

Proposition 1. *When a^L and a^R are defined by $a^L=max(a^{L,1},a^{L,2})$ and $a^R=max(a^{R,1},a^{R,2})$, the waves of the Riemann problem are ordered as follows:*

$$u^L-\frac{a^L}{\rho^L}<u^*=\frac{a^Ru^R+a^Lu^L}{a^L+a^R}-\frac{\pi^R-\pi^L+\sigma_k\kappa_k(\phi_k^R-\phi_k^L)}{a^L+a^R}<u^R+\frac{a^R}{\rho^R}. \tag{20}$$

Therefore, there is a unique solution of the relaxation system (17) which is piecewise constant (see the Fig. 2). The intermediate states $\mathbf{V}^*,\mathbf{V}^{**}$ are defined with the variables $\pi^*,\pi^{**},\alpha_k^*,\alpha_k^{**},\epsilon^*,\epsilon^{**},(\alpha_k\rho_k)^*$ and $(\alpha_k\rho_k)^{**}$ given by:

$$\pi^*=\pi^L-a^L(u^*-u^L),\quad \pi^{**}=\pi^R-a^R(u^R-u^*),\quad \frac{1}{\alpha_k^*\rho_k^*}=\frac{1}{\alpha_k^L\rho_k^L}+\frac{u^*-u^L}{a^L},\quad \frac{1}{\alpha_k^{**}\rho_k^{**}}=\frac{1}{\alpha_k^R\rho_k^R}+\frac{u^R-u^*}{a^R},$$
$$\epsilon^*=\epsilon^L+\frac{(\pi^*)^2-(\pi^L)^2}{2(a^L)^2},\quad \epsilon^{**}=\epsilon^R+\frac{(\pi^{**})^2-(\pi^R)^2}{2(a^R)^2},\quad \alpha_k^*=\alpha_k^L-\left(1-\frac{\rho^*}{\rho^L}\right)\left[\alpha_k^L-(\theta_k^L)^2\frac{\alpha_k^L\rho_k^L}{\rho^L}\right],$$
$$\alpha_k^{**}=\alpha_k^R-\left(1-\frac{\rho^{**}}{\rho^R}\right)\left[\alpha_k^R-(\theta_k^R)^2\frac{\alpha_k^R\rho_k^R}{\rho^R}\right]. \tag{21}$$

The characteristic velocities are $u^L-a^L/\rho^L, u^*$ and u^R+a^R/ρ^R. The density $\alpha_k^*\rho_k^*$ and $\alpha_k^{**}\rho_k^{**}$ are positive.

The proof of this proposition is straightforward but with tedious calculations that are not presented.

In order to evaluate the accuracy of this solution, we formally derive some stability properties of the relaxation system in the framework proposed in [8]. The additional variables π,θ_k and Φ_k are expanded in power series of λ as follow

$$\pi=p+\lambda\pi^\lambda+O(\lambda^2),\quad \theta_k^2=r_k^2+\lambda\theta_k^\lambda+O(\lambda^2)\quad\text{and}\quad \Phi_k=\Gamma_k+\lambda\Phi_k^\lambda+O(\lambda^2). \tag{22}$$

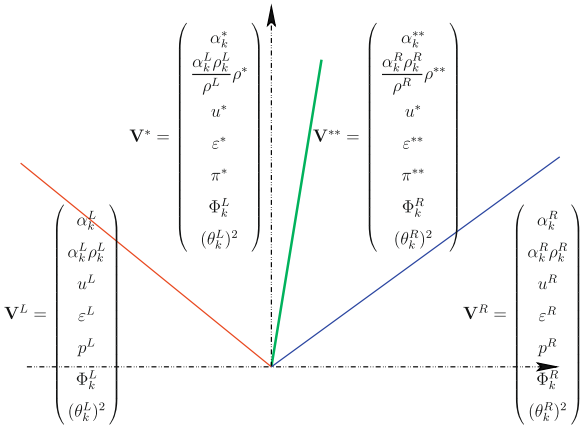

Fig. 2. Solution of the Riemann problem for the relaxation system.

The Chapmann–Enskog method consist of inserting this power series in the relaxation system (17). For the volume fraction equation, this yield to the following equation:

$$\partial_t(\alpha_k) + u\partial_\xi(\alpha_k) + \beta_k\partial_\xi(u) = -z\lambda\frac{\alpha_k\rho_k}{\rho}\partial_\xi(u)[\partial_t + u\partial_\xi]\frac{(\rho c)^2}{(\rho_k c_k)^2},$$

where $z = 1$ for the Kapila model and $z = 0$ for the Massoni model. We assume that derivatives, on the right-hand side of this equation, are smooth. Similar computations are performed to the other equations and, identifying terms of the same power of λ, we end up with the following first-order asymptotic equilibrium system:

$$\partial_t(\mathbf{W}) + \partial_\xi(\mathscr{F}) + \mathscr{B}\partial_\xi(\mathbf{V}) = \lambda\partial_\xi(\mathbf{C}\partial_\xi\mathbf{W}) + z\lambda\mathbf{G}. \tag{23}$$

The vector $\mathbf{G}$ is defined by:

$$\mathbf{G} = (g_{k1}(\partial_\xi\mathbf{u})^2, \quad 0, \quad 0, \quad 0, \quad 0)^T, \tag{24}$$

with $g_{k1} = \frac{\alpha_k(\rho c^2)^2}{\rho_k c_k^2}\left(\frac{\gamma_k+1}{\rho_k c_k^2} - \rho c^2\sum_{k'}\frac{\alpha_{k'}(\gamma_{k'}+1)}{(\rho_{k'}c_{k'}^2)^2}\right)$.

The matrix $\mathbf{C}$ is defined as

$$\mathbf{C} = \begin{pmatrix} 0 & 0 & 0 & 0 & 0 \\ 0 & 0 & 0 & 0 & 0 \\ \frac{2\delta_a}{(\gamma-1)}\frac{\partial p}{\partial\alpha_k} & u(u\delta_a - \delta_b) & -(2u\delta_a - \delta_b) & 2\delta_a & 0 \\ \frac{2u\delta_a}{(\gamma-1)}\frac{\partial p}{\partial\alpha_k} & u^2(u\delta_a - \delta_b) & -u(2u\delta_a - \delta_b) & 2u\delta_a & 0 \\ 0 & 0 & 0 & 0 & 0 \end{pmatrix}, \tag{25}$$

where $\delta_a = (\gamma-1)\frac{(a^R - a^L)}{2\rho}$ and $\delta_b = \frac{a^R a^L - \rho^2 c^2}{\rho^2}$. This matrix $\mathbf{C}$ is positive defined when the condition $a^L a^R > \rho^2 c^2$ is satisfied. Under this constraint, the relaxation scheme is a dissipative approximation of the original system.

As we have derived a relaxation system that approximates accurately the original system, we now propose to derive some properties of the scheme. In particular, it is also easy to show that combinations of the Riemann invariants along shocks make:

$$[\lambda_s\alpha_k\rho_k - \alpha_k\rho_k u] = 0, \quad [\lambda_s\rho u - \rho(u^2 + \pi)] = 0 \quad \text{and} \quad [\lambda_s E - (E + \pi)u] = 0,$$

for $\lambda_s = u - a^L/\rho$ and $\lambda_s = u + a^R/\rho$. Therefore, the mixture density, momentum and total energy of the relaxation solution satisfy Rankine–Hugoniot jump conditions across shocks. For contact discontinuities ($\lambda_s = u$), we have:

$$[\lambda_s\alpha_k\rho_k - \alpha_k\rho_k u] = 0, \quad [u] = 0 \quad \text{and} \quad [\pi + \sigma_k\kappa_k\Phi_k] = 0.$$

The jump of the pressure at the interface is exactly balanced by the capillary effects. The Laplace law is thus recovered.

Using the Rankine–Hugoniot jump relations across discontinuities and identifying the conservative and the non-conservative contributions, we can define the operators $\mathscr{N}$ and $\overline{\mathscr{N}}$ such that:

$$\sum_s \lambda_s(\delta\mathbf{W})_s^{R,L} = \mathbf{F}^R - \mathbf{F}^L + \mathscr{N}(\mathbf{W}^L, \mathbf{W}^R) - \overline{\mathscr{N}}(\mathbf{W}^L, \mathbf{W}^R),$$

where λ_s denotes the sth approximate wave-speed of the solution and $(\delta\mathbf{W})_s$ the associated jump. The non-conservative contribution are defined as

$$\mathscr{N}(\mathbf{W}^L, \mathbf{W}^R) = \overline{\mathbf{B}}^{R,L}\mathbf{V}^R \quad \text{and} \quad \overline{\mathscr{N}}(\mathbf{W}^L, \mathbf{W}^R) = \overline{\mathbf{B}}^{R,L}\mathbf{V}^L,$$

with:

$$\overline{\mathbf{B}}^{R,L} = \begin{pmatrix} u^* & 0 & \frac{Z_k^R a^R + Z_k^L a^L}{a^R + a^L} & \frac{(Z_k^R - Z_k^L)}{a^R + a^L} & \frac{\sigma_k\kappa_k(Z_k^R - Z_k^L)}{a^R + a^L} \\ 0 & 0 & 0 & 0 & 0 \\ 0 & 0 & 0 & 0 & \sigma_k\kappa_k \\ 0 & 0 & 0 & 0 & \sigma_k\kappa_k u^* \\ 0 & 0 & 0 & 0 & u^* \end{pmatrix}, \tag{26}$$

with $Z_k = \alpha_k - (\theta_k)^2\frac{\alpha_k\rho_k}{\rho}$. Therefore, under the CFL condition, we can derive a stable and efficient approximate Riemann solver for the present non-conservative hyperbolic system. The associated non-conservative fluctuations $\boldsymbol{\psi}^{R,L}$ and $\boldsymbol{\psi}^{L,R}$, respectively on the right and on the left of the interface, are

$$\boldsymbol{\psi}^{R,L} = \frac{1}{2}\left[\mathbf{F}^R + \mathbf{F}^L + \mathscr{N}(\mathbf{W}^L, \mathbf{W}^R) - \overline{\mathscr{N}}(\mathbf{W}^L, \mathbf{W}^R) - \sum_s |\lambda_s|(\delta\mathbf{W})_s\right]$$

and $\boldsymbol{\psi}^{L,R} = \boldsymbol{\psi}^{R,L} - \mathscr{N}(\mathbf{W}^L, \mathbf{W}^R) + \overline{\mathscr{N}}(\mathbf{W}^L, \mathbf{W}^R)$. The derived scheme is then composed of an usual upwind flux for the conservative part and an additional component that avoids the difficulty related to "consistent discretization the non-conservative

contributions". The existence of a matrix $\overline{\mathbf{B}}^{R,L}$ was assumed in [13] and evaluated for specific non-conservative systems where the Roe linearization can be generalized.

3. Low mach preconditioning

One of the crucial requirement of multi-fluid algorithms is the ability to accurately span a wide range of multi-fluid conditions, from fully compressible to the low Mach regimes. The low Mach number setting is a singular asymptotic in compressible flows. This flow regime is characterized by a large discrepancy between the magnitude of the acoustic wave-speed and the flow velocity. The usual time-marching solvers for compressible flow are not able to compute nearly incompressible flows. Indeed, they may suffer from severe stability and accuracy deficiencies and, without modification, become inefficient for the low Mach number limit [21,43]. Using an expansion of primitive variables in power of Mach number, it has been shown that numerical problems arising at low Mach regimes are due to the lack of accuracy in the density-based approximation of the pressure field [41,40]. To cure these drawbacks, modification of the numerical viscosity was successfully applied. The main ingredient is based on the fact that the incompressible Euler system is not a natural vanishing Mach limit of the compressible model [4]. Indeed, in the low Mach asymptotic, the compressible model contains both an oscillatory (acoustic) and a slowly varying (incompressible limit) component.

In the present paper, preconditioning is obtained by the introduction of an acoustic fluctuation characteristic time τ, associated to "incompressible" pressure, smaller than the mean flow characteristic time. Time-marching solutions are then designed from pseudo acoustic-waves obtained by altering time-derivatives of the pressure. This is similar to the procedure used in the pseudo-time (or dual-time) [40,43,11,41] and pseudo compressibility [34] approaches. In this context, the sub-scale evolution of the pressure is then given by:

$$\partial_\tau p + u\partial_\xi p + \rho c^2 \partial_\xi u = 0 \quad \text{where} \quad \tau \equiv tM^2,$$

and M is the Mach number. This sub-scale evolution of the pressure will give a proper filtering for low Mach regime. The preconditioned system is:

$$\begin{cases} \partial_t(\alpha_k) + u\partial_\xi(\alpha_k) + \beta_k \partial_\xi(u) = 0, \\ \partial_t(\alpha_k\rho_k) + u\partial_\xi(\alpha_k\rho_k) + \alpha_k\rho_k\partial_\xi(u) = 0, \\ \partial_t(u) + u\partial_\xi(u) + \frac{1}{\rho}\partial_\xi(p) = -\frac{\sigma_k\kappa_k}{\rho}\partial_\xi(\Gamma_k), \\ \partial_t(p) + M^2 u\partial_\xi(p) + M^2\rho c^2\partial_\xi(u) = 0, \\ \partial_t(\Gamma_k) + u\partial_\xi(\Gamma_k) = 0. \end{cases} \tag{27}$$

In order to design a preconditioned relaxation solver, the linearized pressure is now governed by the following equation:

$$\partial_t(\pi) + u\partial_\xi(\pi) + \frac{a^R - a^L}{\rho}\partial_\xi(\pi) + \frac{a^R a^L}{\rho}\partial_\xi(u) = 0,$$

where a^L and a^R are two positive reals which magnitudes must obey:

$$\frac{a^R a^L}{\rho} \approx M^2\rho c^2 \quad \text{and} \quad \frac{a^R - a^L}{\rho} \approx (M^2 - 1)u. \tag{28}$$

Therefore, $-a^L$ and a^R can be approximated by the root of the second order polynomial $x^2 + (M^2-1)ux - M^2\rho c^2$:

$$\begin{aligned} a^R &\approx \frac{\rho}{2}\left(\sqrt{(M^2-1)^2u^2 + 4c^2M^2} + (M^2-1)u\right), \\ a^L &\approx \frac{\rho}{2}\left(\sqrt{(M^2-1)^2u^2 + 4c^2M^2} - (M^2-1)u\right). \end{aligned} \tag{29}$$

The preconditioned relaxation system still write under the same form than the relaxation system (17). The analytical expression of the solution do not change, the difference only comes from the values of a^L and a^R.

Using the Chapman–Enskog expansions (22), we found that the preconditioned relaxation system equilibrium is a dissipative approximation of the preconditioned system. The equilibrium system writes under the form (23) where the dissipative matrix $\mathbf{C}$ is of the form (25), with coefficients δ_a and δ_b now defined as:

$$\delta_a = \frac{\gamma - 1}{2}\left(\frac{a^R - a^L}{\rho} - (M^2-1)u\right) \quad \text{and} \quad \delta_b = \frac{a^R a^L - M^2\rho^2c^2}{\rho^2}.$$

The vector $\mathbf{G}$ is now given by:

$$\mathbf{G} = (g_{k1}(\partial_\xi \mathbf{u})^2 + g_{k2}(\partial_\xi \mathbf{u})(\partial_\xi p), \quad 0, \quad 0, \quad 0, \quad 0)^T, \tag{30}$$

with:

$$\begin{cases} g_{k1} = \frac{\alpha_k(\rho c^2)^2}{\rho_k c_k^2}\left(\frac{M^2\gamma_k+1}{\rho_k c_k^2} - \rho c^2 \sum_{k'} \frac{\alpha_{k'}(M^2\gamma_{k'}+1)}{(\rho_{k'}c_{k'}^2)^2}\right), \\ g_{k2} = \frac{\alpha_k \rho c^2 (M^2-1)u}{\rho_k c_k^2}\left(\frac{\gamma_k}{\rho_k c_k^2} - \rho c^2 \sum_{k'} \frac{\alpha_{k'}\gamma_{k'}}{(\rho_{k'}c_{k'}^2)^2}\right). \end{cases}$$

The matrix $\mathbf{C}$ is positive defined when:

$$a^L a^R > M^2 \rho^2 c^2. \tag{31}$$

This inequality is very complementary to Eq. (28). Thus, it can be made compatible with the approximate values of a^R and a^L given by the relations (29).

The relaxation system is not, a priori, stable when the reals a^L and a^R are chosen following (31) and (29). In fact, the filter devised for the pressure equation demands the consideration 'well prepared' initial conditions. Additional conditions are also required to make sure that a physically admissible solution exist. They are given in the Proposition 1.

3.1. Regularized interface functions and approximate interface curvature

The numerical approximation of the surface tension force is linked to the design of a regularized function Γ_k that maps out the interface delimiting the materials k. This function is defined under regularity and spatial localization constraints. In practice, the interface function Γ_k is computed by using a level set indicator associated to the fluid variables that vary across the interface: (α_k, y_k and ρ for instance). More generally, an approximation of the type $\Gamma_k = f_k(\mathbf{W}(x))$ can be used. Unfortunately, the sprawl of $f_k(\mathbf{W})$ is governed by the numerical dissipation. In order to avoid this undesirable effect, a free surface capturing and smoothing process has been developed. The capturing process is defined as:

$$H_\zeta(x) = H_\zeta(f_k) = \begin{cases} 1 & \text{if } f_k(\mathbf{W}) > \zeta, \\ 0 & \text{else}, \end{cases}$$

where ζ is an appropriate parameter. The interface function Γ_k is then obtained by the regularization of $H_\zeta(f_k)$:

$$\Gamma_k(x, t^n) = \Gamma_k(\mathbf{W}^n) = \int H_\zeta(x) G(x) dx,$$

where G is a regularization kernel with compact support defining a transition layer.

The approximate curvature $(\kappa_k)_i$ associated to each control volume C_i is evaluated by reformulating the divergence operator present in (10) with the Green relation:

$$(\kappa_k)_i = \frac{1}{a_i}\int_{C_i} \nabla\cdot\left(\frac{\nabla\Gamma_k}{|\nabla\Gamma_k|}\right)d\mathbf{x} = \frac{1}{a_i}\int_{\partial C_{i,j}} \frac{\nabla\Gamma_k}{|\nabla\Gamma_k|}\cdot\mathbf{n}ds \approx \frac{1}{a_i}\sum_{j\in v(i)}\left(\frac{\nabla\Gamma_k}{|\nabla\Gamma_k|}\right)_{i,j}\cdot\mathbf{n}_{i,j},$$

where $(\nabla\Gamma_k/|\nabla\Gamma_k|)_{i,j}$ is an evaluation of the normal at the segment $\partial C_{i,j}$. We suppose that this quantity follows the relation:

$$\left(\frac{\nabla\Gamma_k}{|\nabla\Gamma_k|}\right)_{i,j} = \mu_k\left(\frac{\nabla\Gamma_k}{|\nabla\Gamma_k|}\right)_i + (1-\mu_k)\left(\frac{\nabla\Gamma_k}{|\nabla\Gamma_k|}\right)_j,$$

where $(\nabla\Gamma_k/|\nabla\Gamma_k|)_i$ is calculated from the approximate gradient $(\nabla\Gamma_k)_i$:

$$(\nabla\Gamma_k)_i = \frac{1}{a_i}\int_{C_i}\nabla\Gamma_k dx \approx \sum_{\tau\in\tau(i)}\frac{a_\tau}{3a_i}\nabla\Gamma_k|^\tau.$$

The parameter μ_k is set in order to prevent large numerical errors when the curvature evaluation is singular (Γ_k closed to 0 or 1). Numerical results obtained for academic configurations show relatively accurate computations of the interface normal (Fig. 3) and curvature (Fig. 4).

3.2. Implicit scheme

At the low Mach regime, an implicit scheme is unavoidable to obtain a stable numerical scheme. Let us recall the explicit scheme for the relaxation solver:

$$\mathbf{W}_i^{n+1} = \mathbf{W}_i^n - \frac{\Delta t}{a_i}\sum_{j\in\vartheta(i)}\psi_{i,j}(\mathbf{W}_i^n, \mathbf{W}_j^n),$$

where the numerical flux $\psi_{i,j}(\mathbf{W}_i, \mathbf{W}_j)$ is defined as:

$$\psi_{i,j}(\mathbf{W}_i, \mathbf{W}_j) = \frac{1}{2}[\mathbf{F}(\mathbf{W}_i) + \mathbf{F}(\mathbf{W}_j) + \mathcal{N}(\mathbf{W}_i, \mathbf{W}_j) - \overline{\mathcal{N}}(\mathbf{W}_i, \mathbf{W}_j) - \sum_s |\lambda_s(\mathbf{W}_i, \mathbf{W}_j)|(\delta\mathbf{W})_s(\mathbf{W}_i, \mathbf{W}_j)].$$

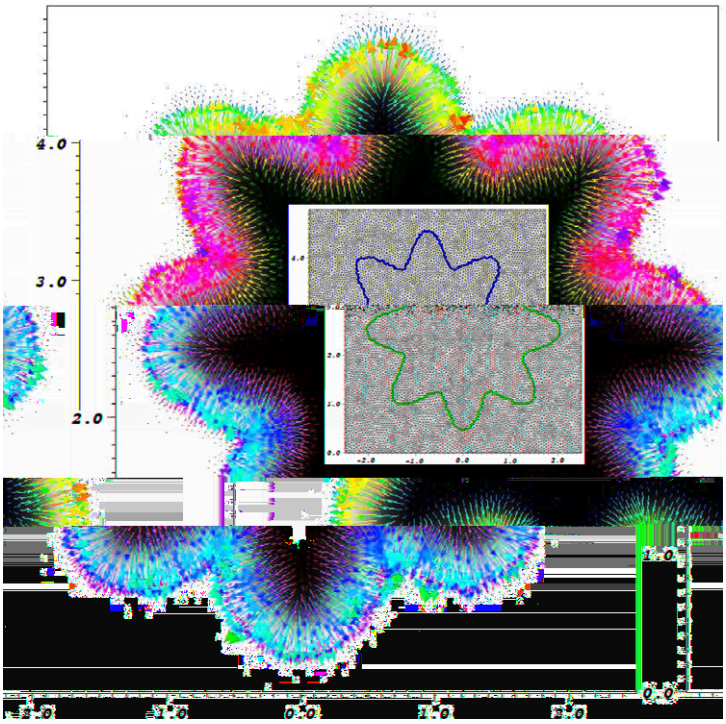

Fig. 3. Interface $f_k(\mathbf{W}) = \zeta$, regularized function Γ_k and interface normal $\nabla\Gamma_k$.

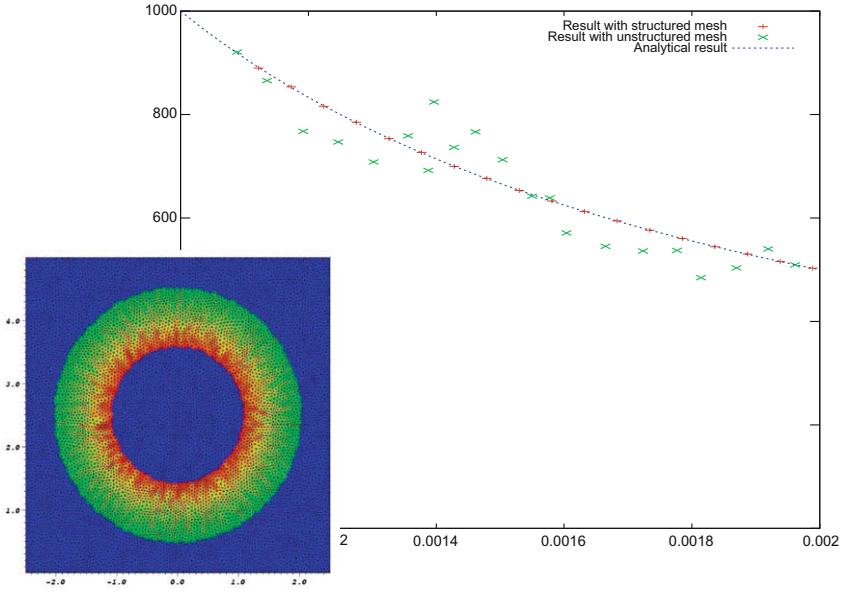

Fig. 4. Curvature approximation on structured and unstructured meshes. Analytical (dot line) and computed (+ and $\times$) curvature as functions of the radius.

The functions $\mathbf{F}(\mathbf{W})$, $\mathbf{V}(\mathbf{W})$, $\mathcal{N}(\mathbf{W}, \mathbf{W}_*)$, $\overline{\mathcal{N}}(\mathbf{W}, \mathbf{W}_*)$, $\lambda_s(\mathbf{W}, \mathbf{W}_*)$ and $(\delta\mathbf{W})_s(\mathbf{W}, \mathbf{W}_*)$ defining the numerical flux are given and derivable. The implicit scheme is obtained from an evaluation of the numerical flux $\psi_{ij}(\mathbf{W}_i, \mathbf{W}_j)$ at the time t^{n+1}:

$$\mathbf{W}_i^{n+1} = \mathbf{W}_i^n - \frac{\Delta t}{a_i} \sum_{j \in \vartheta(i)} \psi_{ij}(\mathbf{W}_i^{n+1}, \mathbf{W}_j^{n+1}). \tag{32}$$

Therefore, $\mathbf{W}^{n+1}$ is the solution of a large sparse nonlinear system. Newton–Krylov algorithm is a suitable approach to solve this system. Unfortunately, due to the absolute values in the flux formulation, the Jacobian of the system is not always defined. In practice, a approximate Jacobian of the numerical flux is assumed, such as for $m = i$ or $m = j$:

$$\frac{\partial \boldsymbol{\psi}_{i,j}}{\partial \mathbf{W}_m} \simeq \frac{1}{2}\left[\frac{\partial \mathbf{F}}{\partial \mathbf{W}_m} + \frac{\partial \mathcal{N}}{\partial \mathbf{W}_m} - \frac{\partial \overline{\mathcal{N}}}{\partial \mathbf{W}_m} - \sum_s |\lambda_s(\mathbf{W}_i, \mathbf{W}_j)| \frac{\partial (\delta \mathbf{W})_s}{\partial \mathbf{W}_m}\right]. \tag{33}$$

A linear system is then computed and solved at each Newton iteration. This is achieved by preconditioned (ILU) iterative solvers: Jacobi, Gauss–Seidel, Gmres. An efficient and scalable parallel sparse direct solver, based on a LU factorization, has also been used [25].

Let us denote by $\boldsymbol{\psi}^{(1)}_{i,j}(\mathbf{W}_i, \mathbf{W}_j)$ and $\boldsymbol{\psi}^{(2)}_{i,j}(\mathbf{W}_{i+}, \mathbf{W}_{j-})$ respectively the first and second order accurate scheme where $\mathbf{W}_{i+}$ and $\mathbf{W}_{j-}$ are the reconstructed and limited values obtained by the MUSCL approach. The second order implicit scheme uses the following approximation of the Newton step:

$$\frac{a_i}{\Delta t}\delta \mathbf{W}_i + \sum_{j\in\vartheta(i)}\left[\left(\frac{\partial \boldsymbol{\psi}^{(1)}_{i,j}}{\partial \mathbf{W}_i}\right)^n \delta \mathbf{W}_i + \left(\frac{\partial \boldsymbol{\psi}^{(1)}_{i,j}}{\partial \mathbf{W}_j}\right)^n \delta \mathbf{W}_j\right] = -\frac{\Delta t}{a_i}\sum_{j\in\vartheta(i)} \boldsymbol{\psi}^{(2)}_{i,j}\left(\mathbf{W}^n_{i+}, \mathbf{W}^n_{j-}\right),$$

where $\delta \mathbf{W} = \mathbf{W}^{n+1} - \mathbf{W}^n$ are the unknowns. When only one step of the Newton method is performed, it is the usually called "linearized implicit scheme".

4. Numerical results

4.1. Multi-material shock tubes (1D)

In order to validate the proposed relaxation scheme, let us consider a 1D multi-material shock tube problem where the materials under consideration are assumed to be perfect gas characterized by different adiabatic indexes. The results are compared with the exact solution. Two test cases are performed for initial conditions with large density (10 and 400) and pressure (2500 and 1000) ratios [26]. Figs. 5 and 6, are obtained for the Kapila model ($\beta_k \neq 0$), with an explicit scheme and numerical flux computed by the relaxation scheme. The waves are in the proper localization and there is no spurious waves at the material interface. Indeed the velocity (and of course the pressure also, but not plotted) is constant across the material interface. Similar results are also obtained when $\beta_k = 0$. The other test cases proposed in [26] has been successfully performed in [10].

4.2. Shock bubble interactions

Let us consider the shock bubble interaction experiments driven by Hass and Sturtevant [22] and computed numerically in [36]. These experiments involve strong acoustic effects. The surface tension forces, the viscous effects and the gravity are not considered. The computational domain is a $[0, 30\text{ cm}] \times [0, 10\text{ cm}]$ rectangle. The initial condition is a bubble of radius 3.5 cm centered at (5 cm,5 cm), at the equilibrium in the air and a plane shock characterized by the Mach number $M_S = 1.22$ localized at $x = 0$ cm. The air is initially at rest:

$$\rho = 1.0, \quad u = 0, \quad v = 0, \quad p = 1.0, \quad \gamma = 1.4.$$

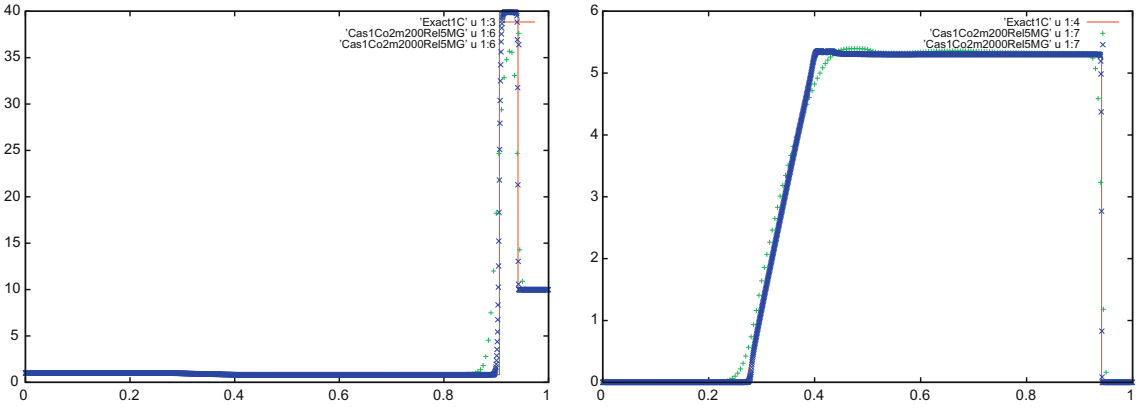

Fig. 5. Two fluid shock tube problem solved by a second order accurate relaxation scheme. Computed density (left) and velocity (right) at the time $T = 0.03$ with meshes of 200 and 2000 points. The initial interface is localized at $x = 0.8$. On the left: $\rho_L = 1,\ u_L = 0,\ p_L = 500$ and $\gamma_L = 1.4$. On the right: $\rho_R = 10,\ u_R = 0,\ p_R = 0.2$ and $\gamma_R = 1.667$.

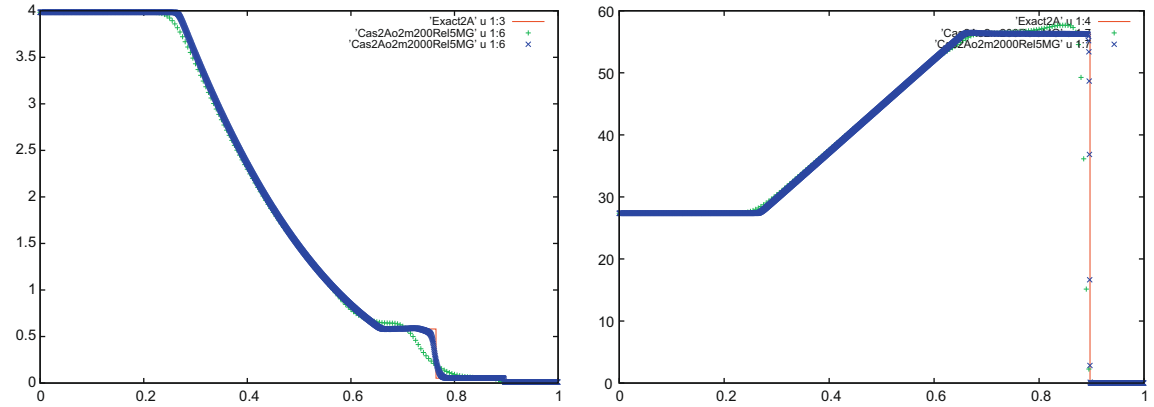

Fig. 6. Two fluid shock tube problem solved by a second order accurate relaxation scheme. Computed density (left) and velocity (right) at the time $T = 0.01$ with meshes of 200 and 2000 points. The initial interface is localized at $x = 0.2$. On the left: $\rho_L = 3.984,\ u_L = 27.355,\ p_L = 1000$ and $\gamma_L = 1.667$. On the right: $\rho_R = 0.01,\ u_R = 0,\ p_R = 1$ and $\gamma_R = 1.4$.

The incoming shock is then defined by the following conditions at the left boundary of the computational domain:

$$\rho = 3.4, \quad u = 2.14, \quad v = 0, \quad p = 7.48, \quad \gamma = 1.4.$$

Computations are performed for the Kapila model ($\beta_k \neq 0$) using an explicit relaxation scheme. Mesh size is 2401×801 points and the numerical system is of 11.5 millions unknowns. In order to use modern computer architectures, we have developed a SPMD (Single Program Multiple Data) parallel strategy based on mesh partitioning and the message passing interface (MPI). The computations have been performed with 64 processors.

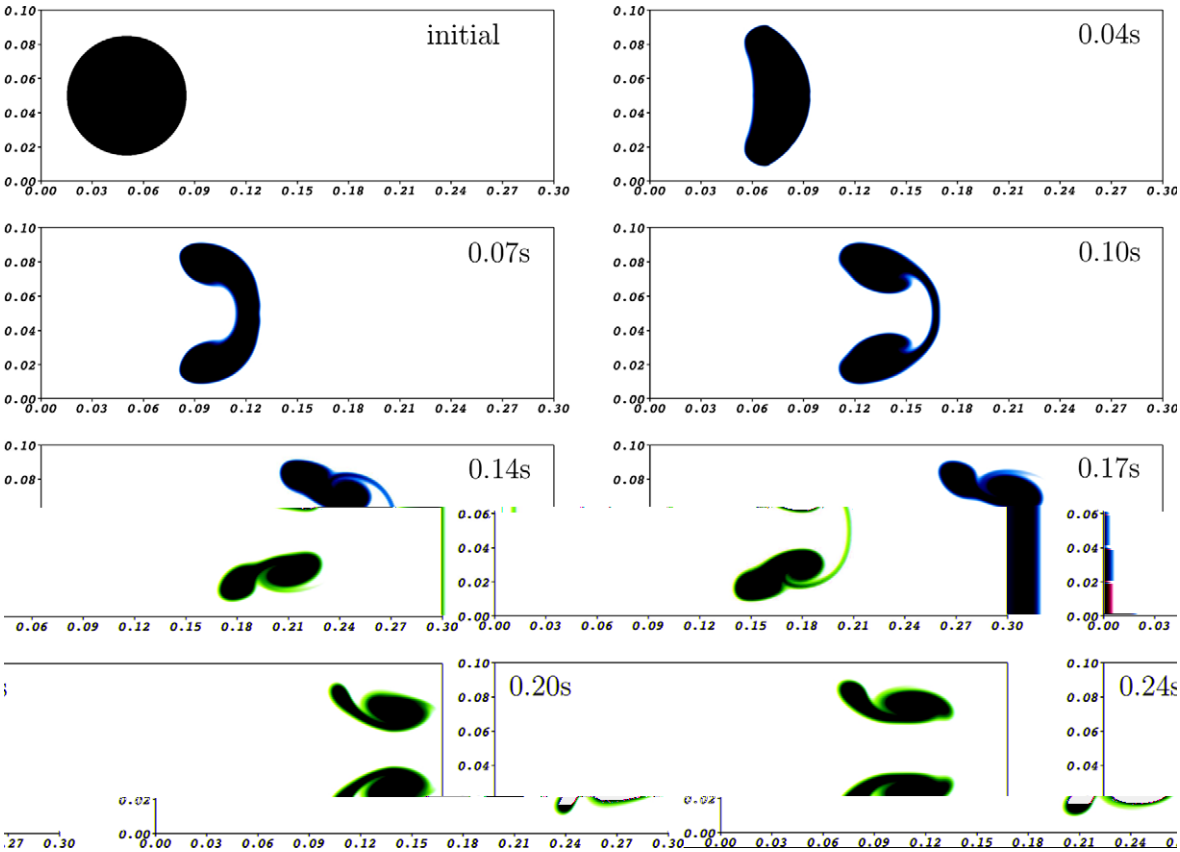

Fig. 7. Computations (2D) of a shock interaction with an helium bubble in the air: evolution of the helium volume fraction, explicit relaxation solver.

Numerical computations are performed for two gas bubbles [22], respectively for helium ($\rho_{He} = 0.138$ and $\gamma = 1.6$) and for the R22 refrigerant gas ($\rho_{R22} = 3.154$ and $\gamma = 1.25$). In the two cases, the numerical results agree with the experimental results given by Haas and Sturtevant [22]. Let us recall that as the helium bubble is lighter, it acts as a convergent media for the acoustic-waves. For the refrigerant R22, as the bubble is heavier, it is a divergent media. The entire numerical results are displayed in the Figs. 7 and 8.

4.3. Laplace law

The Laplace law gives a relation, at the equilibrium, between the pressure jump and the surface tension force strength at the material interface: $\Delta p = \sigma\kappa$, where σ is the surface tension coefficient and κ the interface curvature. For a water/air interface, we have $\sigma = 0.073$ in the SI units. In order to recover numerically this property, let us consider an initial spherical water drop of square section (edge of 3 cm). Evolution of this drop can be computed by the 2D axisymmetrical formulation. Gravity forces are not considered in this case, such that, at the equilibrium the bubble is a spherical water drop and the pressure jump satisfies the Laplace law. Computations performed with a second order accurate preconditioned relaxation scheme (Fig. 9) shows that the numerical behavior is in accordance with the considered physics. The parasitic currents are under control, the equilibrium is obtained numerically and the Laplace law is satisfied (Fig. 10). This validates the numerical strategy based on the CSF formulation and relaxation method for the computation of tension forces.

4.4. Dynamic of a water drop in the air, under gravity and surface tension forces

This computation almost uses the same physical features given in [35]. It consists of a falling water drop under gravity and surface tension forces. This is a low Mach regime flow and the usual finite volume approximation fails at this asymptotic. In order to overcome this difficulty, in [35], a scaling is performed: "*For computational convenience, the drop radius is taken equal to* 0.25 m. *According to the Bond number, we adjust surface tension coefficient,* $\sigma = 175$ N/m, *where gravity acceleration g is taken equal to* 25 m/s^2".

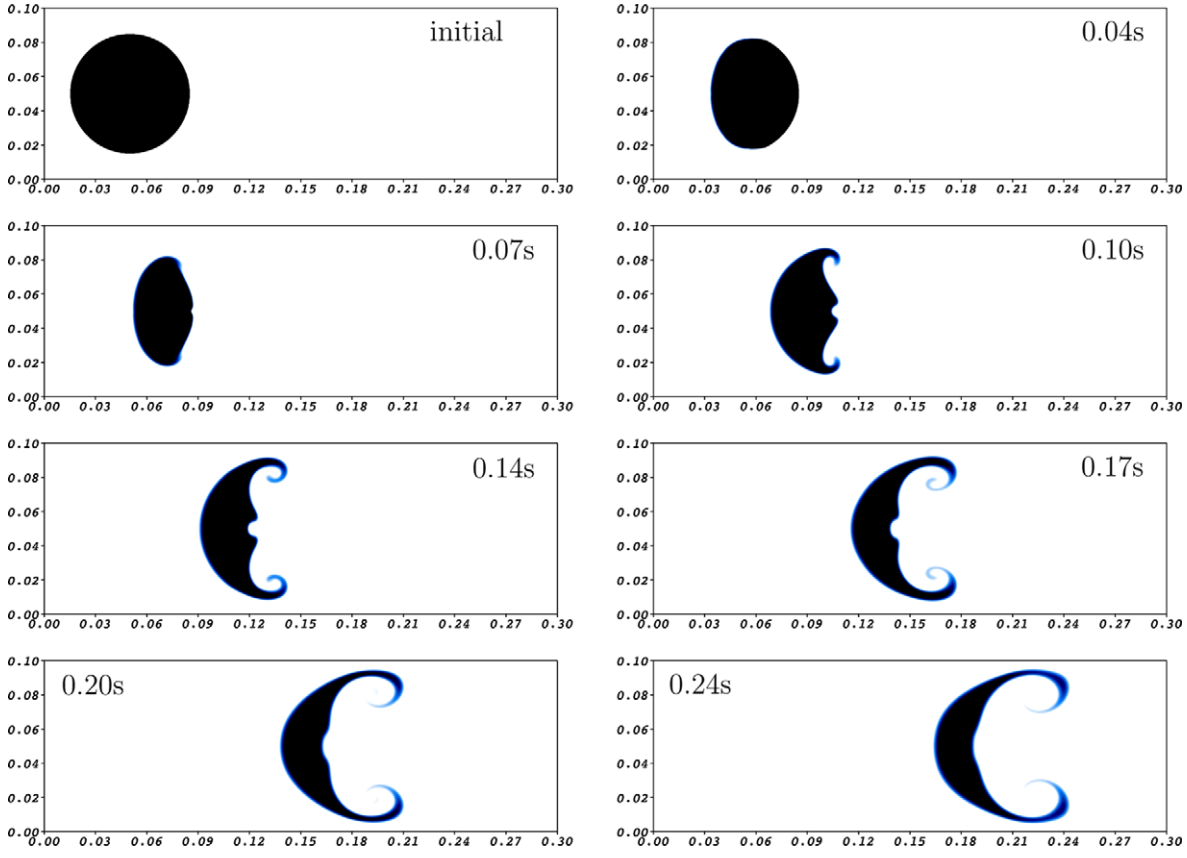

Fig. 8. Computations (2D) of a shock interaction with an R22 refrigerant bubble in the air: evolution of the R22 refrigerant volume fraction, explicit relaxation solver.

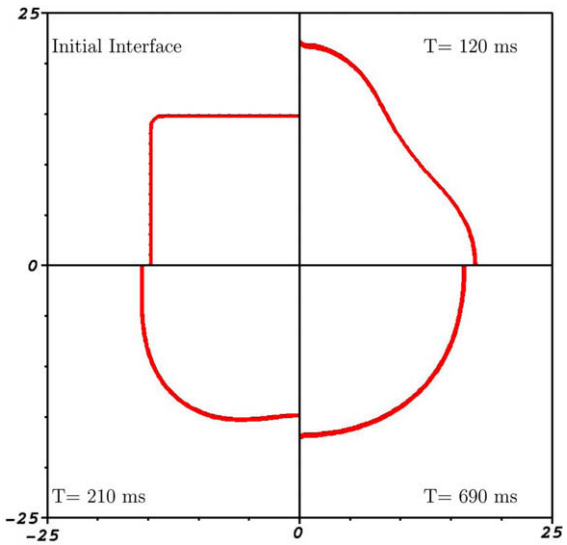

Fig. 9. Evolution and equilibrium of an interface under surface tension force: Laplace law.

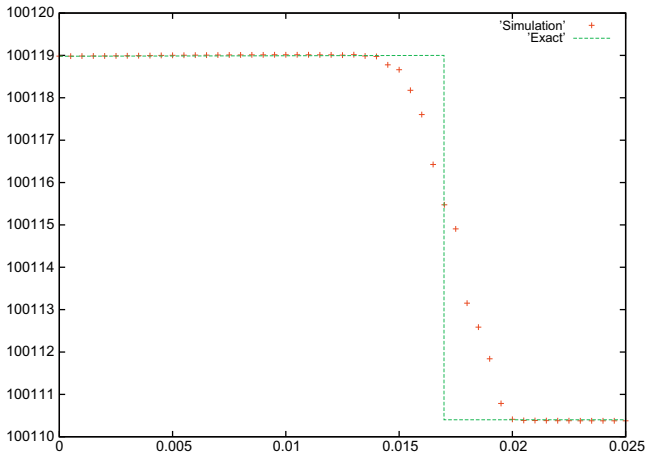

Fig. 10. Pressure as a function of the radius. The relaxation method associated to the CSF approximation of the surface tension force recovers the Laplace law $\delta p = 2\sigma/r = 2\frac{0.073}{r}$.

In the present context, low Mach preconditioning technique combined with an implicit second order accurate scheme allows the use of physical values without any rescaling. We assume axisymmetrical property of the flow and consider a 2D rectangular computational domain $[0, 0.025\ \text{m}] \times [0, 0.1\ \text{m}]$. The mesh size is 101×401. Initially, a half spherical water bubble of radius $r = 0.006$ m is centered at $(0.0, 0.1)$ m. Water is also present in the computational domain for $y \leqslant 0.01$ m (Fig. 11: Initial). The gravity is set to $g = -10\ \text{m/s}^2$ and the initial conditions for air and water are given by:

	ρ (kg m^{-3})	$\mathbf{u}$ (m/s)	p (Pa)	p^∞ (Pa)	γ	μ (m^2 s^{-1})
Air	1	0	10^5	0	1.4	1.86×10^{-6}
Water	1000	0	10^5	6×10^8	4.4	10^{-3}

The contact angle is set to 25°. This is the reason why the initial plane water interface is not stable (see Fig. 11). For this computations, the drop velocity is $\simeq 1$ m/s, the speeds of sound are 374 m/s in the air and 1625 m/s in the water. Therefore, the Mach number is about 6×10^{-4} and the preconditioning technique is unavoidable.

As the gravity forces are greater than the surface tension, the water drop falls with the structure of a liquid jet. The quantity of falling liquid depends of the surface tension value. The liquid jet divides in four small bubbles which impact the liquid

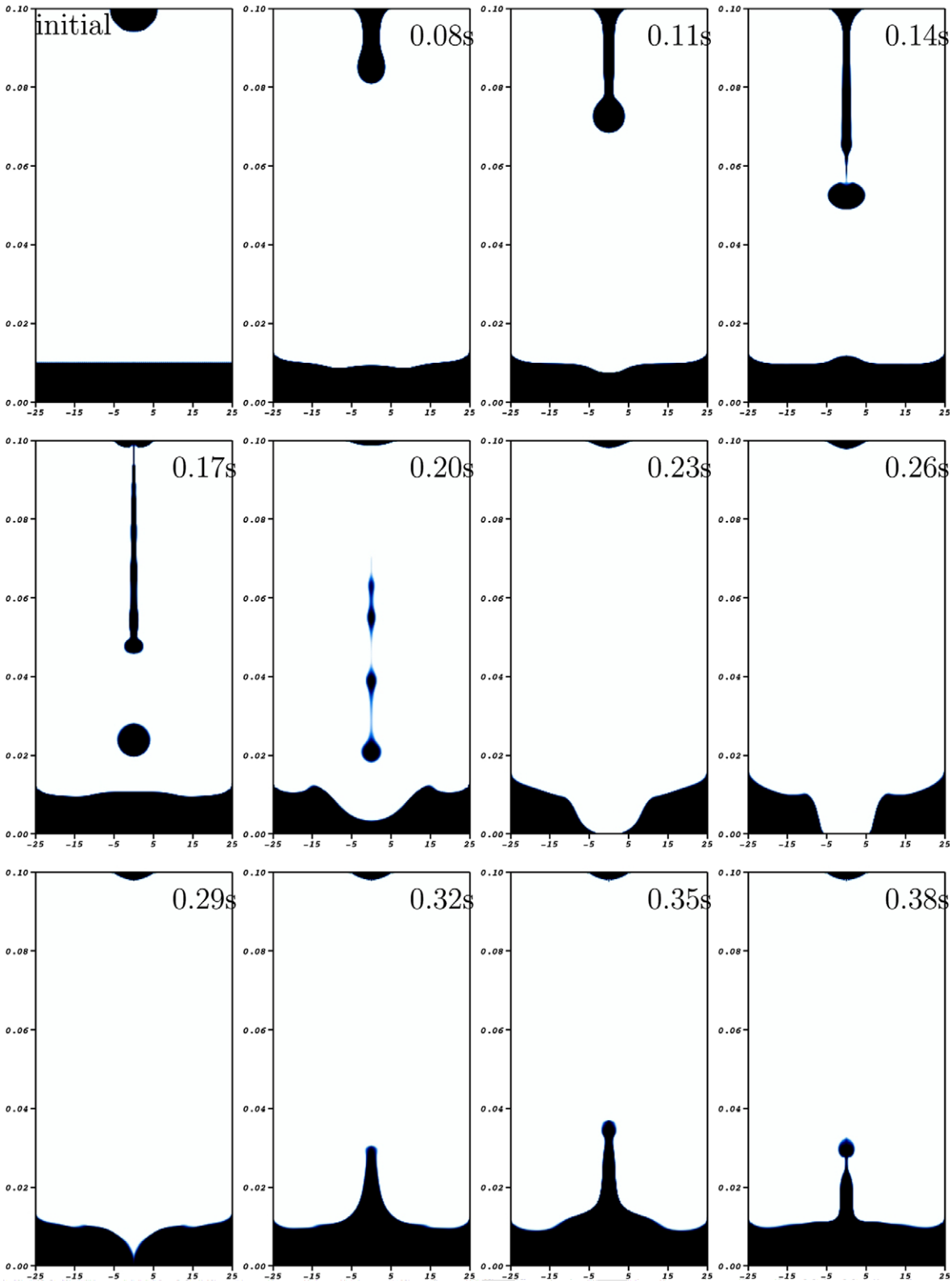

Fig. 11. 2D Axisymmetric viscous flow computations of water drop in air, falling and splashing into water, under effects of gravity and surface tension forces. 25 mm $\times$ 100 mm length domain, $\simeq$40,000 mesh vertices. Second order accurate (MUSCL) preconditioned implicit relaxation solver.

surface on the base of the domain. We then observe the propagation of surface waves that after reflection on the wall, form a vertical liquid jet. This behavior is in agreement with physical observations [35].

5. Conclusion

In the present work, we have exhibited a new numerical method to approximate the solution of mono-velocity mono-pressure diffuse interface multiphase models including surface tension forces in their CSF formulation. Our procedure, based on the relaxation scheme, allows a consistent resolution of the non-conservative and conservative terms present in the model and prevents the generation spurious waves. In particular, interfaces submitted to surface tension and governed by the Laplace law are explicitly recovered by our numerical scheme. Then, identifying the physical time scales associated to material and acoustic-waves, we succeed in deriving, in a new manner, a numerical scheme devoted to the resolution of low Mach number flows. Our approach is based on the preconditioned relaxation procedure. The resulting numerical scheme allows to reproduce standard experiments: shocks tube, shock bubble interactions. Finally, this scheme, in its implicit version, has been used to resolve the difficult experiment of the liquid break up without modifying its physical features.

The future work will be devoted to the resolution of 3D problems. For this, the accuracy of our method needs to be improved at the interfaces by, for instance, the use of mesh adaptive methods.

Acknowledgments

This work has been partially supported by the Commissariat à l'Énergie Atomique, by the French/Taiwan program ORCHID Grant of the National science council of Taiwan NSC 97-2911-1-002-015 and EGIDE (France) and by INRIA Futurs (projet ScAlApplix). The authors would also like to address special thanks to Christophe Berthon (Université de Nantes) and to Jean Claudel (CEA CESTA) for their support and precious advices.

References

[1] R. Abgrall, How to prevent pressure oscillations in multicomponent flow calculations: a quasi conservative approach, J. Comput. Phys. 125 (1996) 150–160.
[2] R. Abgrall, S. Karni, Computations of compressible multifluids, J. Comput. Phys. 169 (2) (2001) 594–623.
[3] R. Abgrall, R. Saurel, A multiphase Godunov method for compressible multifluid and multiphase flows, J. Comput. Phys. 150 (1999) 425–467.
[4] T. Alazard, Low Mach number limit of the full Navier–Stokes equations, Arch. Ration. Mech. Anal. 180 (1) (2006) 1–73.
[5] M.R. Baer, J.W. Nunziato, A two-phase mixture theory for the deflagration-to-detonation transition (DDT) in reactive granular materials, Int. J. Multiphase Flows 12 (1986) 861–889.
[6] M. Baudin, C. Berthon, F. Cocquel, R. Masson, Q.H. Tran, A relaxation method for two-phase flow models with hydrodynamic closure law, Numer. Math. 99 (2005) 411–440.
[7] C. Berthon, B. Braconnier, B. Nkonga, Numerical approximation of a degenerated non-conservative multifluid model: relaxation scheme, Int. J. Numer. Methods Fluids 48 (1) (2005) 85–90.
[8] F. Bouchut, Nonlinear Stability of Finite Volume Methods for Hyperbolic Conservation Laws, and Well-balanced Schemes for Sources, Frontiers in Mathematics Series, Birkhauser, 2004.
[9] J.U. Brackbill, D.B. Kothe, C. Zemach, A continuum method for modeling surface tension, J. Comput. Phys. 100 (1992) 335–354.
[10] B. Braconnier, Modélisation numérique d'écoulements multiphasiques pour des fluides compressibles, non miscibles et soumis aux effets capillaires, PhD Thesis, Univeristé Bordeaux 1, 2007.
[11] P.E.O. Buelow, S. Venkateswaran, C.L. Merkle, Stability and convergence analysis of implicit upwind schemes, Comput. Fluids 30 (7–8) (2001) 961–988.
[12] G.Q. Chen, C.D. Levermore, T.P. Liu, Hyperbolic conservation laws with stiff relaxations terms and entropy, Commun. Pure Appl. Math. 47 (1995) 787–830.
[13] P. Cargo, G. Gallice, Roe matrices for ideal MHD and systematic construction of Roe Matrices for systems of conservation laws, J. Comput. Phys. 136 (1997) 446–466.
[14] F. Coquel, B. Perthame, Relaxation of energy and approximate Riemann solvers for general pressure laws in fluid dynamics, SIAM J. Numer. Anal. 35 (1998) 2223–2249.
[15] R. Fedkiw, T. Aslam, B. Merriman, S. Osher, A non-oscillatory Eulerian approach to interfaces in Multimaterial flows (the ghost fluid method), J. Comput. Phys. 152 (2) (1999) 157–192.
[16] P. Le Floch, G. Dalmaso, F. Murat, Definition and weak stability of non-conservative products, J. Math. Pures Appl. 74 (1995) 483–548.
[17] J. Glimm, J. Grove, X. Li, D. Tan, Robust computational algorithms for dynamic interface tracking in three dimensions, SIAM J. Sci. Comput. 21 (6) (2000) 2240.
[18] D. Gueyffier, J. Li, A. Nadim, R. Scardovelli, S. Zaleski, Volume-of-fluid interface tracking with smoothed surface stress methods for three-dimensional flows, J. Comput. Phys. 152 (1999) 423–456.
[19] H. Guillard, A. Murrone, A five equation reduced model for compressible two phase flow problems, J. Comput. Phys. 202 (2) (2005) 664–698.
[20] H. Guillard, A. Murrone, On the behavior of upwind schemes in the low Mach number limit. 2: Godunov type schemes, Comput. Fluids 33 (4) (2004) 655–675.
[21] H. Guillard, C. Viozat, On the behavior of upwind schemes in the low mach number limit, Comput. Fluids 28 (1) (1999) 63–86.
[22] J.F. Haas, B. Sturtevant, Interaction of a weak shock wave with cylindrical and spherical gas inhomogeneities, J. Fluid Mech. 181 (1987) 41–76.
[23] B.T. Hayes, P. G LeFloch, Non-classical shocks and kinetic relations: strictly hyperbolic systems, SIAM J. Math. Anal. 139 (1997) 1–56.
[24] T.Y. Hou, P. Le Floch, Why non-conservative schemes converge to the wrong solution: error analysis, Math. Comput. 62 (206) (1994) 497–530.
[25] P. Hénon, P. Ramet, J. Roman, PaStiX: a high-performance parallel direct solver for sparse symmetric definite systems, Parallel Comput. 28 (2) (2002) 301–321.
[26] X.Y. Hu, B.C. Khoo, An interface interaction method for compressible multifluids, J. Comput. Phys. 198 (2004) 35–64.
[27] D. Jamet, D. Torres, J.U. Brackbill, On the theory and computation of surface tension: the elimination of parasitic currents through energy conservation in the second-gradient method, J. Comput. Phys. 182 (2002) 262–276.
[28] S. Jin, Z.P. Xin, The relaxation schemes for systems of conservation laws in arbitrary space dimensions, Commun. Pure Appl. Math. 48 (1995) 235–278.
[29] A.K. Kapila, R. Menikoff, D.S. Stewart, Two-phase modeling of deflagration to detonation transition in granular materials: reduced equations, Phys. Fluids 13 (2001) 3002–3024.

[30] P.G. LeFloch, Entropy weak solutions to non-linear hyperbolic systems under non conservation form, Commun. Part. Diff. Eq. 13 (1988) 669–727.
[31] T.P. Liu, Hyperbolic conservation laws with relaxation, Commun. Math. Phys. 108 (1987) 153–175.
[32] M. Lutz, B. Nkonga, P. Jack, J. Claudel, Application of the ghost fluid methods for interfaces flows, in: ENUMATH, Graz, 2007.
[33] J. Massoni, R. Saurel, B. Nkonga, R. Abgrall, Proposition de méthodes et modèles eulériens pour les problèmes à interfaces entre fluides compressibles en présence de transfert de chaleur, J. Heat Mass Transfer 45 (6) (2001) 1287–1307.
[34] R. Nourgaliev, T.G. Theofanous, High-fidelity interface tracking in compressible flows: unlimited anchored adaptive level set, J. Comput. Phys. 224 (2) (2007) 836–866.
[35] G. Perigaud, R. Saurel, A compressible flow model with capillary effects, J. Comput. Phys. 209 (2005) 139–178.
[36] J. Quirk, S. Karni, On the dynamics of a shock–bubble interaction, J. Fluid Mech. 318 (1996) 129–163.
[37] R. Saurel, R. Abgrall, A simple method for compressible multifluid flows, SIAM J. Sci. Comput. 21 (3) (1999) 1115–1145.
[38] R. Scardovelli, S. Zaleski, Direct numerical simulation of free-surface and interface flows, Annu. Rev. Fluid Mech. 31 (1999) 567.
[39] I. Suliciu, Energy estimates in rate-type thermo-viscoplasticity, Int. J. Plast. 14 (1–3) (1998) 224–227.
[40] R.C. Swanson, E. Turkel, Pseudo-time algorithms for the Navier–Stokes equations, Appl. Numer. Math. 2 (1986) 321–333.
[41] S. Venkateswaran, J.W. Lindau, R.F. Kunz, C.L. Merkle, Computation of multiphase mixture flows with compressibility effects, J. Comput. Phys. 180 (1) (2002) 54–77.
[42] E.F. Toro, Riemann Solvers and Numerical Methods for Fluid Dynamics, second ed., Springer-Verlag, 1999.
[43] E. Turkel, Review of preconditioning methods for fluid dynamics, Appl. Numer. Math. 12 (1–3) (1993) 257–284.